Determination of Strain Field on the Superior Surface of Excised Larynx Vocal Folds Using DIC

***Hani Bakhshaee, †Jonathan Young, *Justin C. W. Yang, *Luc Mongeau, and *Amir K. Miri,** *†*Montreal, Quebec, Canada*

Summary: Objective/Hypothesis. The objective of the present study was to quantify the mechanical strain and stress in excised porcine larynges during self-oscillation using digital image correlation (DIC) method. The use of DIC in the excised larynx setup may yield accurate measurements of the vocal fold displacement field.

Study Design. *Ex vivo* animal larynx.

Methods. Measurements were performed using excised porcine larynges on a humidified flow bench, equipped with two high-speed cameras and a commercially available DIC software. Surface deformations were calculated from digital images recorded at 3000 frames per second during continuous self-oscillation for four excised porcine larynges. Larynx preparation consisted of removing the supraglottal wall and the false folds. DIC yielded the deformation field on the superior visible surface of the vocal folds. Measurement data for adducted and freely suspended vocal folds were also used to estimate the distribution of the initial prephonatory strain field. An isotropic constitutive law, the polymer eight-chain model, was used to estimate the surface distributions of planar stresses from the strain data.

Results. The Lagrangian normal strain values were between ∼16% and ∼29% along the anterior-posterior direction. The motion of material points on the vocal fold surface described an elliptical trajectory during oscillation. A phase difference was observed between the anterior-posterior and the medial-lateral component of the displacement. The strain data and eight-chain model yielded a maximum stress of ∼4 kPa along the medial-lateral direction on the superior surface.

Conclusion. DIC allowed the strain field over the superior surface of an excised porcine larynx to be quantified during self-oscillation. The approach allowed the determination of the trajectory of specific points on the vocal fold surface. The results for the excised larynx were found to be significantly different than previous results obtained using synthetic replicas. The present study provides suggestions for future studies in human subjects.

Key Words: Prephonatory strain–Three-dimensional deformation–Digital image correlation (DIC)–Excised porcine larynx–Impact stress–Vocal folds.

INTRODUCTION

Vocal abuse, misuse, and overuse are postulated to be the etiology behind common vocal fold pathologies, including nodules, cysts, and polyps.[1] These benign vocal lesions may cause hoarseness, throat discomfort, and pitch breaks. It is thought that the benign lesions are caused by contact and trauma during normal or pressed phonation.[2] A better understanding of the mechanics of phonation is required to guide the treatment of vocal fold pathologies. To yield this understanding, a detailed knowledge of the mechanical stress and strains during vocal fold vibrations is needed. Mechanical stresses acting on vocal fold tissue during phonation include shear, aerodynamic, tensile, compressive, and inertial stresses. These cause three-dimensional (3D) deformations during vocal fold vibration.[3] Determining the deformation over a surface using a constitutive model allows the calculation of the stress components over that surface. Stress and strain data obtained from experiments on excised larynges can be compared with the corresponding parameters obtained from computer models, which provide a framework for verifying computer simulations.

The mechanical stress associated with the collision of vocal folds is thought to be the strongest contributor to voice trauma.[3] High-impact stresses are believed to cause the formation of nodules, polyps, and cysts; however, the absence of a reliable and an accurate method to measure vocal fold deformations hampers the development of quantitative metrics. Many approaches have been introduced to determine stress and strain fields,[4] including excised larynx experiments,[5–7] physical rubber models,[4,8] human *in vivo* measurements,[9–11] and finite element-based simulations.[12–14] For instance, Jiang and Titze[5] measured impact stresses using surface pressure measurements in excised canine hemilarynges. Verdolini et al[6] used the electroglottography close quotient, the ratio of the period for which the glottis is closed and the oscillation period, as a noninvasive estimate of vocal fold impact stresses in excised canine larynges. Jiang et al[7] compared vocal fold acceleration with simultaneously measured impact stresses. The second derivative of the photoglottography data was used to obtain vocal fold acceleration, which is thought to be proportional to impact stress. A pressure transducer was placed between the vocal folds during phonation to measure the impact stress at the midglottal location.[7] In another study, digital image correlation (DIC) was used to determine the strain field on the superior surface of a self-oscillating physical replica of the human vocal folds.[4] The superior surface strains along with a Hertzian contact

Accepted for publication May 21, 2013.

From the *Department of Mechanical Engineering, McGill University, Montreal, Quebec, Canada; and the †Department of Otolaryngology-Head and Neck Surgery, McGill University, Montreal, Quebec, Canada.

Address correspondence and reprint requests to Amir K. Miri, McGill University, 817 Sherbrooke Street West, Montreal, QC H3A 0C3, Canada. E-mail: amir.miriramsheh@mail.mcgill.ca or akmiri@gmail.com

Journal of Voice, Vol. 27, No. 6, pp. 659-667
0892-1997/$36.00

http://dx.doi.org/10.1016/j.jvoice.2013.05.009

model were used to estimate the distribution of the contact pressure on the medial surface.[4] This method has not been used in human subjects because of the difficulties in creating a speckle pattern on human vocal folds using nontoxic and tolerable substances. Chen and Mongeau[8] used a probe microphone to directly measure the pressure in the contact region between colliding synthetic silicone replicas of the human vocal folds. A finite element model of the replica was created, and the results were compared with both empirical results and predicted results from a Hertzian impact model.

The present study aims to develop an accurate, easy-to-use, and noninvasive method for the measurement of the displacement field over the superior surface of vocal fold tissue. An excised larynx test bench, equipped with two high-speed digital cameras for optical measurements and a regulated airflow supply, was used. Four porcine larynges (n = 4) were used in flow-induced and self-oscillation experiments. The vocal fold surface was covered with a speckle pattern made of graphite powder. The 3D deformation field on the superior surface of the vocal folds was then determined from recorded digital images using DIC. Vocal folds are initially under tension within the laryngeal framework. As customary in excised larynx studies, tension was applied on the vocal folds using known weights to yield a physiologically realistic self-oscillation. The prephonatory strain, hereinafter called "initial strain," causes a bias in the overall strain field. A dissection protocol was introduced and used in the experiments to evaluate the initial strain field. The kinematics of the vocal folds was then investigated to study the vibratory characteristics, homogeneity of the deformation, and time dependency of the displacement components. Finally, an estimation of the impact stress was obtained using the effective strain field—that is, the summation of the relative strain calculated from DIC and the initial strain—and an eight-chain constitutive model adapted from previous studies on polymers.[15]

METHODS

Sample preparation

Porcine larynges were obtained from a local abattoir and transported to the laboratory while immersed in a 0.9% saline solution. A 3-cm long section of the trachea attached to the larynx was kept to facilitate connection to the airflow pipe. A standard snap-freezing protocol was used while each larynx was submerged in normal phosphate saline buffer. On the day of the experiment, they were thawed at room temperature. Then, the surrounding connective soft tissues were removed, and the superior part of the larynx, above the false folds, was dissected as shown in Figure 1A. This was performed by cutting the thyroid cartilage along the midline, up to the level of the false folds, and then laterally to both left and right sides along the dashed lines in Figure 1A. The false folds, shown in Figure 1B, were subsequently removed using small scissors to expose the vocal folds, as shown in Figure 1C. The epiglottis, which is located in the posterior glottis, was removed completely. A thin string was passed through the arytenoid cartilage laterally as suggested by Alipour and Jaiswal.[16] This string was attached to a pulley-weight system

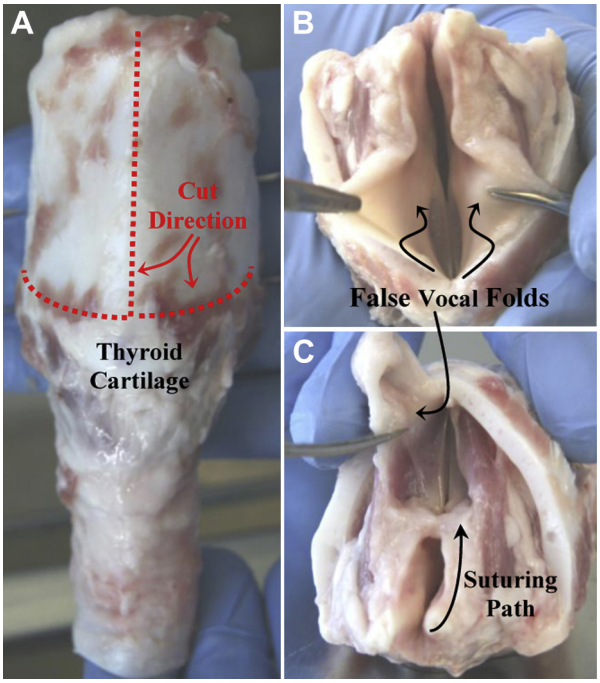

FIGURE 1. Dissection of porcine larynx. **A.** Dash lines show the direction of dissection on the thyroid cartilage. **B.** False folds in porcine larynx. **C.** Cutting the false folds to reveal the vocal folds.

that was designed to pull the arytenoids anteriorly (Figure 2). The tension required for proper oscillation was applied using some known weights. The large gap in the posterior glottis was sealed using surgical sutures beginning at the upper arytenoid and continuing to the most posterior part of the vocal folds, as shown in Figure 1C.

Experimental apparatus

A test frame (80/20 Inc., Columbia City, IN) was mounted on an optical table (ThorLabs, Newton, NJ) to install and stabilize the sample holder, digital cameras, and light source (Figure 2). The system was assembled using aluminum bars (T-slotted profiles), plastic sliders, steel bolts, and Plexiglas plates. The body frame was made of transparent Plexiglas to facilitate the connection between the larynx and the tubes. The cylindrical sample holder had four adjustable screws with flat heads to maintain the larynx. The trachea was glued to a polyvinyl chloride (PVC) tube (McMaster-Carr, Chicago, IL) with an outer diameter of 0.0127 m (1/2′) or 0.0159 m (5/8′), depending on the size of the larynx, to mount the larynx on the test bench. Two screw bars were placed on the posterior part of the folds. The pulley-weight system and screw bars were used to apply the tension required to start self-oscillation. A sutured larynx attached to the pulley-weight system and the sample holder are shown in Figure 2. Any motion of the larynx support could move the region of interest out of the camera's optical focus. To minimize vibrations in the cameras and sample holder, the camera and sample holder frames were rigidly fixed to the optical table.

Two high-speed black and white cameras (Fastcam MC2—Model 10 K; Photron Limited, San Diego, CA) were installed

on the frame using adjustable sliders. Their position could be changed along three spatial directions. Images were obtained at a rate of 3000 frames per second to obtain sufficient temporal resolution. Higher frame rates decreased the field of view, and 3000 frames per second was the highest rate at which the region of interest was completely captured by cameras. A distance of 40 cm between the vocal folds and the cameras was found to provide an optimum field of view. The cameras were equipped with two zoom lenses (EF-S17-85 mm; Canon Canada, Mississauga, ON), which allowed for increased optical resolution. A fiber optic light (Model 21-AC; Salem, NH) with two semirigid probes was located approximately 8–10 cm away from the vocal fold surface to produce sufficient light. The light beam was oriented at an angle of approximately 30° with respect to the horizontal axis to minimize glare. Other components of the experimental setup are shown schematically in Figure 3.

A centrifugal blower (D-14.5 cm; Ametek Windjammer, Kent, OH) was used as the airflow source. A muffler was used to attenuate flow fluctuations from the flow supply. Airflow was humidified and heated up to 90–95% and 30–37°C, respectively, using a heated humidifier (HC-150; Fisher & Paykel, Mississauga, ON). The time-averaged mean volumetric flow rate was measured using a flow meter (MKS Instruments, Andover, MA). The static pressure was also recorded at a 1–2 cm distance before the trachea using a hydrostatic pressure transducer (MKS Instruments, Andover, MA). Once the larynx was secured in the holding clamp and attached to the PVC tubing, the flow rate was increased until the onset of self-oscillation. Typical shapes of the mean subglottal pressure versus flow rate are shown in Figure 4. Measurements were performed while increasing and decreasing flow rate to capture hysteresis. The pressure recorded while the flow rate was decreased was consistently lower than that recorded while the flow rate was increased. Such a trend was observed for all larynges tested and is consistent with results from Alipour and Jaiswal[17] during pressure sweep experiments on porcine larynges.

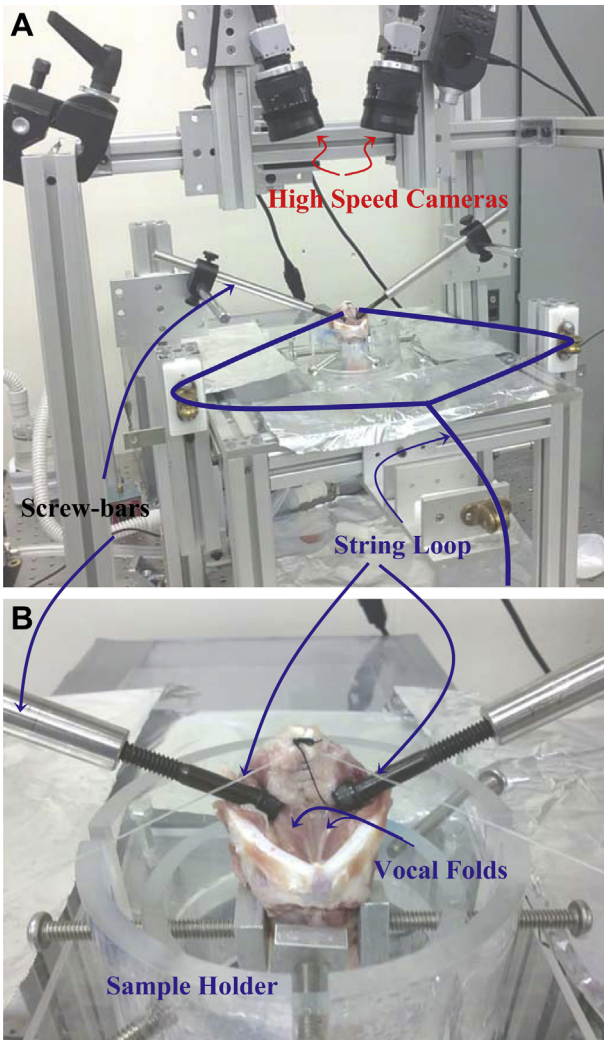

FIGURE 2. **A.** Excised larynx setup. **B.** Larynx holder.

Digital image correlation

DIC analyses were performed using the commercially available VIC-3D and VIC-2D softwares (Correlated Solutions, Inc., Colombia, SC). DIC yields surface displacements along three spatial directions from correlations of grayscale patterns between a reference image and successive deformed images. A randomized speckle pattern was applied on the deformable solid to uniquely identify each material point. As multiple pixels may have the same grayscale value, the program analyzes a square subset of pixels of predetermined size and calculates the strain as the square is deformed. More details about the algorithm used can be found in the literature.[15,18]

Different dyes were tested to create a robust speckle pattern with a good adhesion onto the tissue surface, without diffusion or dispersion. Isotropic diffusion of the dye creates a uniform color distribution, inappropriate for the unique identification of subset in the images. In addition to chemical dyes, cosmetic products, such as foundation sprays and ink powders, as well as food dyes were tested. Powdered dyes such as methylene blue and congo red were tested with multiple solvents, including water, corn syrup, and barium. Many produced insufficient contrast or produced a uniform coating rather than local speckles. Contact with humidified air and collision between vocal folds tended to displace or entirely remove the dye. Drying for nearly 30 minutes did not resolve the problem. The best results were obtained using a cosmetic facial product and graphite powder. A thin layer of foundation material was sprayed on the vocal fold surface. Graphite powder was then sprinkled over the foundation layer. Solid particles of graphite powder do not diffuse in the tissue, and they reduce glare. The typical area of interest for DIC analysis and the coordinate system with the origin in the center of the imaged area are shown in Figure 5. The x-axis and y-axis are oriented along the medial-lateral and the anterior-posterior directions, respectively. The selected area approximately included the middle half of the vocal folds' length (from $-L/4$ to $+L/4$) along the y-direction, where L is the anterior-posterior length. The areas near the anterior and posterior ends (ie, $y > L/4$ and $y < -L/4$) were excluded from the area of interest for DIC because of the low vibration amplitude in these regions. Figure 5 also shows the contour of surface height along the inferior-superior direction (ie, the z-axis).

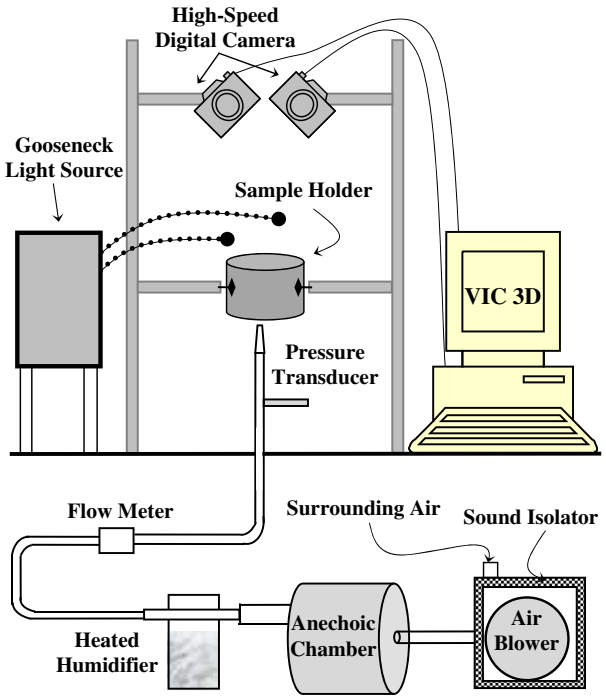

FIGURE 3. Schematic drawing of the excised larynx setup.

Determination of the initial prephonatory strain

Vocal folds are initially under tension before phonation onset. To prevent mode changes and frequency jumps,[17] which is a very common phenomenon for porcine larynges, further tension was applied to adjust pitch and obtain a self-sustained oscillation using the pulley-weight system and screw bars. To estimate the effective strains and stresses, the initial strain must be added to the relative strain measured during vibration. The following approach was used to obtain the initial strain field. After recording high-speed images of the vocal folds during self-sustained oscillation, a snapshot of the vocal folds in the resting position (ie, with no airflow) was recorded. Using a scalpel, a half-circle circumferential cut was made starting at anterior end of the vocal folds to remove them from the thyroid cartilage. This was done to remove any strain caused by the natural geometry of the vocal folds within the laryngeal cartilage framework. The cutting path and dissected tissue are shown in Figure 6A, where weights and the screw bars were removed. Efforts were made to maintain the orientation of the larynx and preserve the speckle pattern. In some cases, the vocal folds moved out of the optical focus of the cameras, hampering DIC analysis. Vocal fold images at rest and after dissection were imported into VIC-3D and VIC-2D to calculate the initial at-rest strain. The dissected vocal fold image was used as the reference image to measure the initial strain. The image of the vocal fold at rest was used as the reference image to measure strain during phonation.

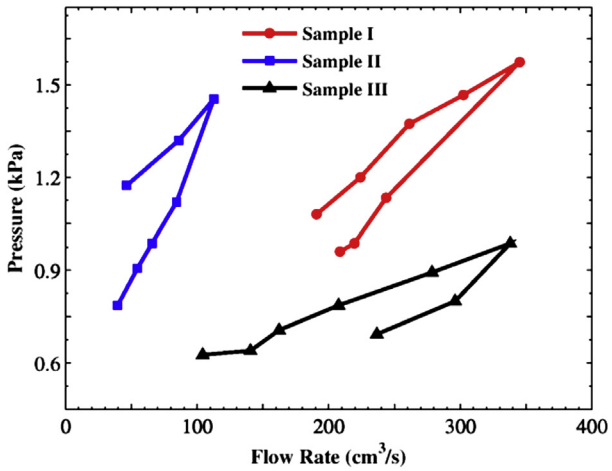

FIGURE 4. Pressure versus flow rate for three porcine larynges (samples I, II, and III).

RESULTS AND DISCUSSION

Initial strain field on the vocal folds

The initial strain deformation of the vocal fold surface was evaluated. Because of inhomogeneity through the thickness of the vocal fold tissue, from the epithelium to the muscle, the strains mostly indicate the deformation of the superficial lamina propria.[15] More than 10 larynges were subjected to the initial prephonatory strain protocol. When vocal folds were subjected to the prephonatory dissection protocol, some of the larynges were moved out of camera's focus and as a result were excluded from DIC analyses. In some cases, the vocal folds fell down after removal, and their position and speckle pattern were changed dramatically, causing a low image correlation. These large displacements could not be captured by 3D DIC, and 2D DIC was used instead. Only one sample yielded an acceptable correlation range for 3D DIC, as four samples supplied proper images for 2D planar DIC.

One typical image of the area of interest in VIC-2D is shown on the superior surface of the vocal folds in Figure 6. The distributions of the initial strain in the medial-lateral direction, ε_{0xx}, and anterior-posterior direction, ε_{0yy}, on the vocal fold surface before removal from the thyroid cartilage are shown in Figure 6B and C, respectively. The measured strain values were relatively larger in the center of the imaged area. The initial strain values, ε_{0xx}, ε_{0yy}, and ε_{0xy}, in the central region of the vocal fold for four samples are shown in Table 1. As expected, the initial strain along the anterior-posterior direction, ε_{0yy}, had the largest magnitude. The normal strains along the x-direction

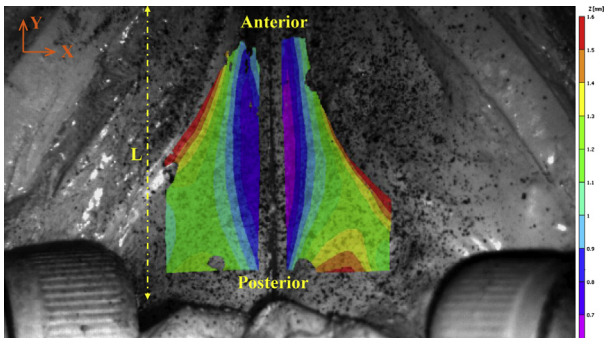

FIGURE 5. Porcine vocal folds with a layer of speckle pattern with the contour of depth position on the superior surface of vocal fold. (Z-axis is directed vertically upward, and $Z = 0$ is the image plane).

are positive, implying a tensile initial strain in the vocal folds. Variability in the initial strain magnitudes may be because of the unavoidable differences in suturing, larynx size, and weights used to obtain self-sustained oscillation. The calculated initial strains are consistent with visual observations. Removal caused tissue shrinkage posteriorly with a large deformation. Both vocal folds moved toward the midsagittal plane, showing a tensile initial strain in both the anterior-posterior and medial-lateral directions.

Kinematics of vocal fold vibrations

The kinematics of the self-oscillations during the opening and closing phases of the glottal cycle were investigated. The flow rate, static pressure, and frequency of vibration were $Q = 236\ \text{cm}^3/\text{s}$, $P = 690$ Pa, and $f = 245$ Hz, respectively. Comparisons were made with previous results obtained using a synthetic replica.[4]

The history of vocal fold displacement for 10 cycles of the tissue vibration at the midpoint, along three spatial directions, is shown in Figure 7A. The medial-lateral displacement amplitude, *U*, was the largest followed by the inferior-superior displacement, *W*. The anterior-posterior displacement amplitude, *V*, had the lowest magnitude, as expected.

A phase difference between displacement components *U* and *W* is observed in Figure 7A. Because of the phase difference between *U* and *W*, material points undergo an elliptical motion over time. To better illustrate this, the vocal fold midpoint trajectory in the frontal plane (*x*–*z* plane) is shown in Figure 7B along with an elliptical regression. The elliptical trajectory of vocal fold material points has been reported in the literature.[19,20] In some synthetic models, there is no phase difference between the medial-lateral and inferior-superior displacements[4]; the physical points reach their maximum and minimum amplitudes in the medial-lateral and inferior-superior directions simultaneously. This highlights limitations of homogeneous physical replicas to produce physiologically realistic oscillation. More realistic physical replicas with larger structures, epithelial-like covers, and in some cases tension control appear to be more realistic with elliptical surface point motion.

The in-plane medial-lateral relative strain at the instant of maximum opening and closure is shown in Figure 8. The initial strain values are neglected in this figure, and only the effect of oscillation on the strain field of the superior surface of the vocal folds is considered. Tensile strain is dominant during closure; the vocal folds were under compressive strain in the fully open state. During closure, the ε_{xx} strain is almost uniform along the edge and anterior-posterior direction. In the open state, the strain reaches a maximum value near the midpoint of anterior-posterior points because of their high displacement amplitude in the *x*-direction.

The time history of the effective strain distribution at the midpoint along the medial-lateral direction, ε_{xx}, and along the anterior-posterior direction, ε_{yy}, is shown in Figure 9. It can be seen that ε_{xx} is alternately in compression and tension, and the oscillation amplitude is much larger than that of ε_{yy}. Although the motion is periodic, slight changes in the maximum and minimum amplitudes of ε_{xx} can be seen from cycle to cycle.

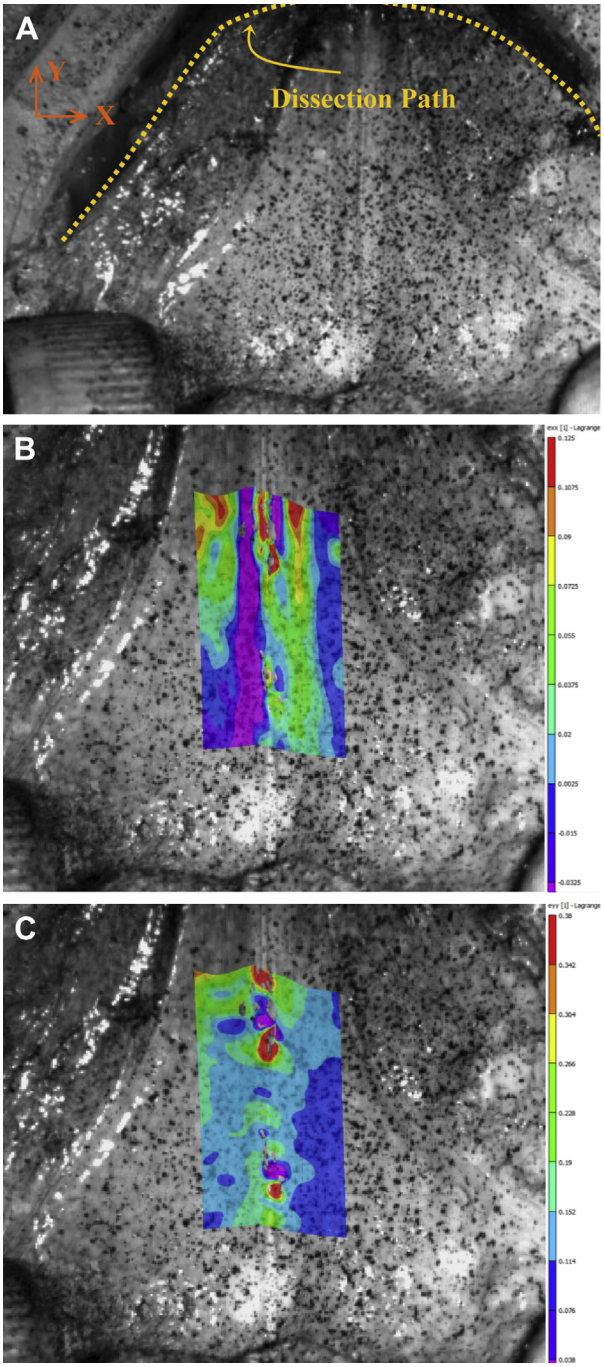

FIGURE 6. **A.** Larynx after cut, showing dissection path. **B–C.** The larynx before cut, displaying prephonatory strain components ε_{xx} and ε_{yy}, respectively.

The anterior-posterior strain, ε_{yy}, was tensile during the entire vibration cycle, with a low oscillation amplitude. The initial strain in the anterior-posterior direction, ε_{0yy}, has a large positive magnitude and superposition of that on the anterior-posterior strain from DIC resulted in the tensile ε_{yy}, over the entire vibration cycle, as shown in Table 1.

Normal strain values at the vocal fold midpoint along the anterior-posterior direction are shown versus flow rate at the time of maximum opening and closure in Figure 10. As seen

TABLE 1.
Initial strains in the Vocal Fold

Sample Number	Length (mm)	ε_{0xx} (%)	ε_{0yy} (%)	ε_{0xy} (%)
1	18.8	3.59 ± 2.18	16.15 ± 2.96	1.57 ± 7.59
2	19.2	7.15 ± 7.68	16.06 ± 4.99	5.59 ± 7.39
3	20.1	10.11 ± 7.44	29.25 ± 4.49	12.27 ± 8.77
4	20.7	7.05 ± 8.59	21.58 ± 9.43	17.72 ± 4.23

before, ε_{xx} is compressive at maximum opening and tensile during the closed phase. For all flow rates presented in this figure, the absolute magnitude of ε_{xx} at maximum opening is larger than that at closing. Vocal folds are near the centerline in the reference image as shown in Figure 5. As a result, less deformation is expected during complete closure than at maximum opening. This behavior of the vocal fold is consistent with that of the synthetic model of Spencer et al.[4] Figure 10B shows values of the anterior-posterior strain ε_{yy} at the midpoint of anterior posterior point versus flow rate. The values of ε_{yy} for closed state decrease as flow rate increases and for maximum opening, the values of ε_{yy} increase with flow rate. The increase rate of ε_{yy} for maximum opening is higher than the decrease rate for closed state.

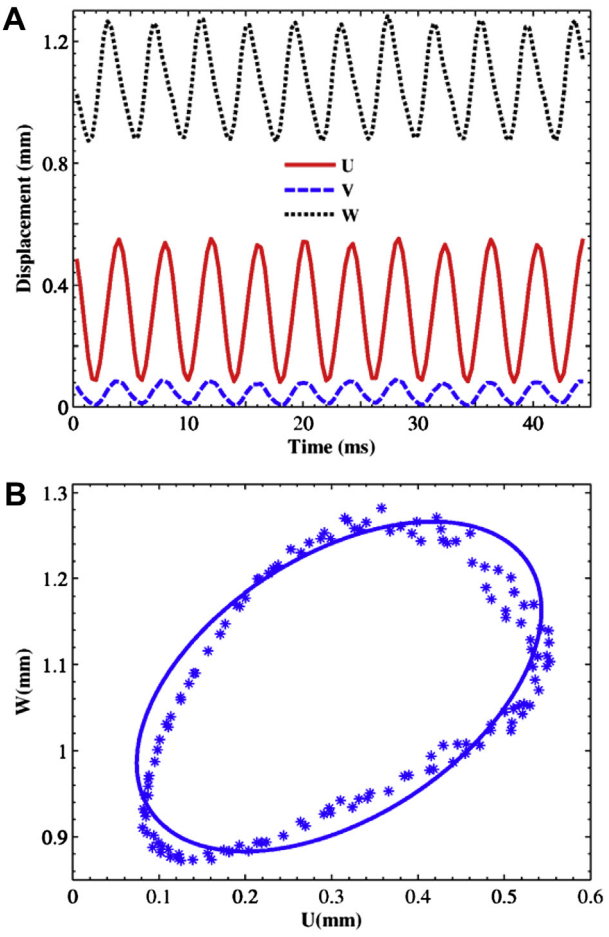

FIGURE 7. **A.** Time history of displacement at the vocal fold midpoint. **B.** Elliptical trajectory of the midpoint.

To correlate strain and displacement, U, W, ε_{xx}, and ε_{yy} are shown over four cycles in Figure 11. To emphasize the phase differences, each variable was normalized by dividing its amplitude by its maximal value. The vocal folds' midpoint was under maximum tensile strain in the medial-lateral direction when it was at the minimum displacement point in the inferior-superior direction. Maximum compressive strain occurred when the midpoint was simultaneously moving in the inferior and lateral directions, away from the location of maximum z- or in x-displacement.

The maximum anterior-posterior tensile strain at the midpoint occurred when (ie, ε_{yy} maximum) the displacement in the inferior-superior direction (ie, W maximum) was also maximum. The maximum compressive strain in the anterior-posterior direction, that is, ε_{yy} minimum, occurred beyond the point of minimum displacement in the medial-lateral direction while motion is in the lateral and superior directions.

Impact stress assessment

The importance of the initial strain field was investigated using an incompressible, isotropic, hyperelastic constitutive law. The well-known eight-chain constitutive model was chosen because the model parameters were obtained from *in vitro* uniaxial traction testing of 10 porcine vocal folds, in a previous study.[15] The application of the model to the strain field of sample 1, with or without adding the initial strain values of Table 1, yields non-traction stress component in the x- and y-directions shown in Figure 12. The distribution of normal stress along the y-direction, based on dynamic strains alone (Figure 12A), is more uniform than for the case with initial strains (Figure 12B) at the closing position. The former has a maximum of ∼1.5 kPa, whereas the latter reaches 15 kPa at some locations. This difference was expected from the difference between corresponding initial strain values (see ε_{0yy} and ε_{0yy} in Table 1) and the hyperelasticity of vocal fold tissue.[15] For the open position of the vocal folds, the stress along the longitudinal direction is tensile and varies between 1 and 15 kPa.

The stress component along the x-direction spanned a symmetric range, from −4 to 4 kPa, when initial strain values were included (Figure 12D), whereas the case of dynamic strains (Figure 12C) spans negative values. The x-stress component can be representative of impact stress because it measures tissue forces along the direction of collision and in a close vicinity of the surface. The compressive stress was 4 kPa for a subglottal pressure of 690 Pa. This stress value is close to the impact stress because of the force equilibrium at the contact point. The value is on the same order of magnitude than impact stresses reported in other studies. In a study by Jiang and Titze,[5]

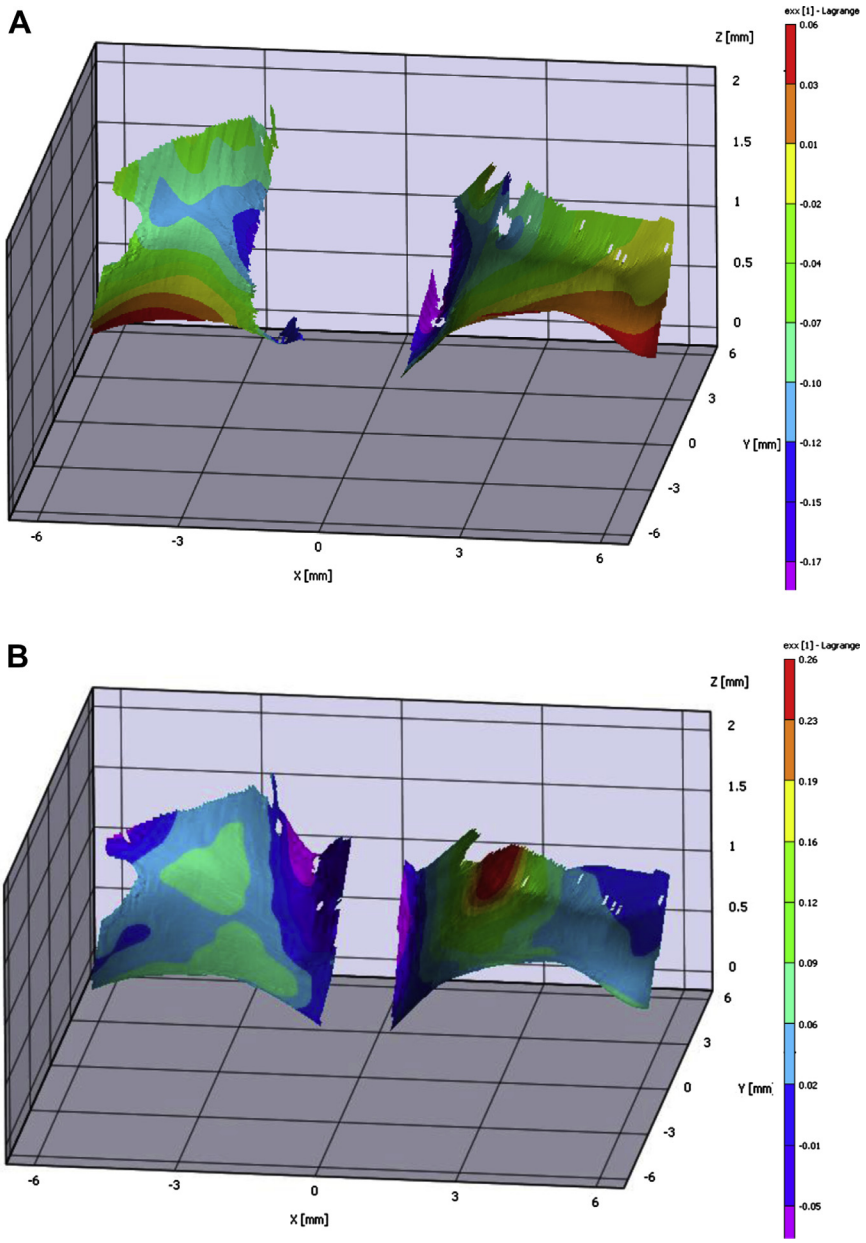

FIGURE 8. Contours of normal strain ε_{xx} on deformed superior surface of vocal fold for **A.** open state and **B.** close state of vocal folds.

the stress between the vocal fold of the canine hemilarynx and the vertical plate was found to be in the range between 0.5 and 5 kPa. Verdolini et al[6] have reported values in the range of 0.3–5.3 kPa for impact stresses of canine larynx. For a subglottal pressure range of 0.9–1.5 kPa, contact pressure ranged from 0.8 to 1.5 kPa in the study by Jiang et al,[7] which is mostly for canine larynges. Considering the subglottal pressure value, the impact stress values in the present study are generally greater than previously reported values.

The normal stress along the transverse direction at closing (Figure 12D) was significantly different than at opening (Figure 12E). During opening, the tissue experiences a compressive stress of 15 kPa near the vocal fold edge. This can be because of aerodynamic stresses (ie, the aerodynamic pressure in the airflow). Stress distributions were calculated using an isotropic model; however, the porcine vocal fold tissue exhibits a strong anisotropy.[21] Future analysis using transverse anisotropic constitution laws[22] will be the object of future studies.

CONCLUDING REMARKS

High-speed imaging, along with DIC, was used to measure the deformation field on the vocal fold surface of porcine larynges during self-sustained oscillation. To calculate the effective strain and stress values, the initial strain field in the vocal folds was calculated. The initial strain originates from the physiology of the laryngeal framework and the exerted force used to make the vocal folds phonate on the excised larynx setup. Empirical findings for the strain field of vocal fold vibrations can be used as the input for computer simulations. Those simulations eventually lead to strategies to reduce stress within the larynx, thus diminishing the incidence of and helping in the nonsurgical therapy of nodules, polyps, and cysts. This may also contribute

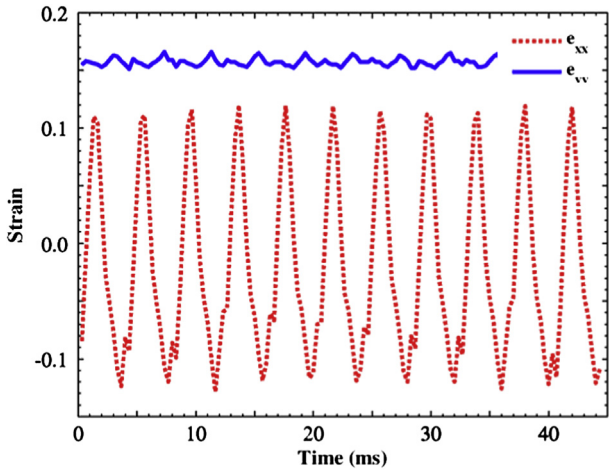

FIGURE 9. Strain-time history at the vocal fold midpoint.

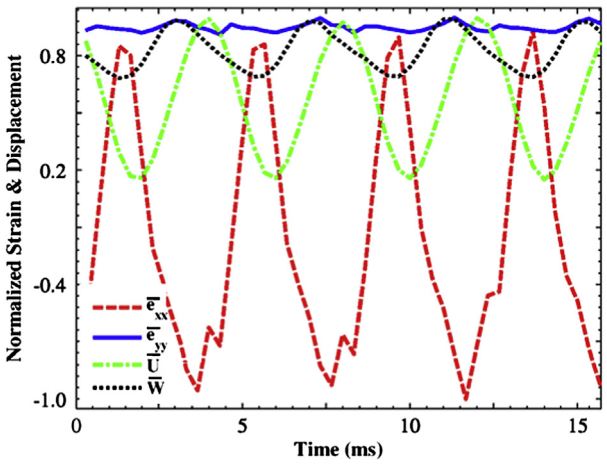

FIGURE 11. Time history of $\varepsilon_{xx}/\varepsilon_{xx,max}$, $\varepsilon_{yy}/\varepsilon_{yy,max}$, U/U_{max}, and W/W_{max} for more than four cycles at the vocal fold midpoint.

to the identification of early lesions, which are difficult to detect clinically.

Although the accuracy of the present methodology was verified by comparing results with laser Doppler velocimetry,[4] a few limitations persist when using it to determine vocal fold deformation fields. Providing a speckle pattern that can remain unchanged on the surface of the vocal folds during oscillation is challenging and time consuming. Even for the optimum combination of background and chemical dye or powder, several trials were needed to obtain the acceptable pattern. Using the backgrounds on the surface of the folds dehydrates the tissue, which may affect its mechanical properties. As a result, the speckle pattern and background were frequently cleaned off during the experiment to hydrate the superior surface of the folds, and a new pattern was then created. For future *in vivo* applications, the speckle pattern must also be nontoxic.

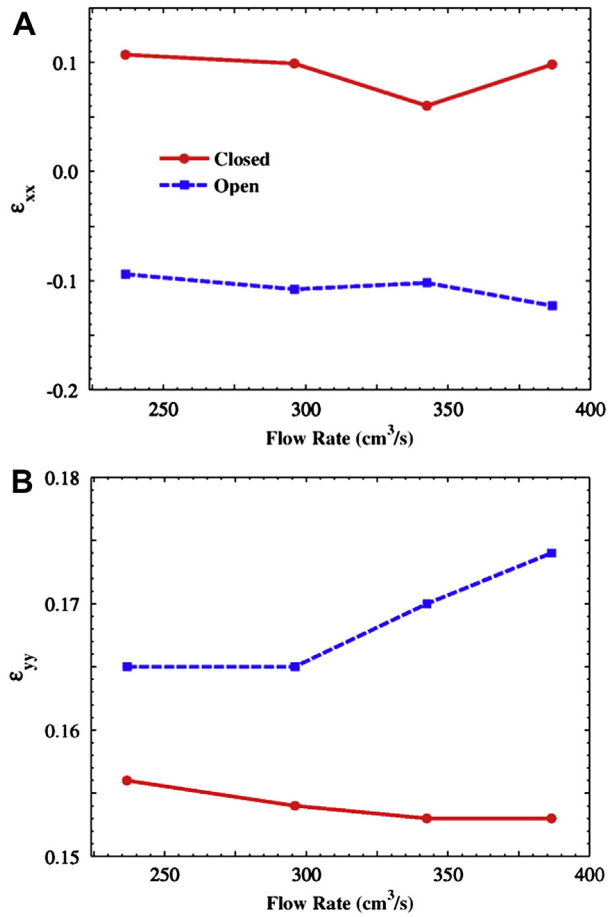

FIGURE 10. Normal strain versus flow rate at the vocal fold midpoint: **A.** ε_{xx} and **B.** ε_{yy}.

Although high-speed cameras provide a high temporal resolution of the displacement and deformation, they have a limited range of optical focus. Slight changes in the location of the larynx or high-amplitude vibration of the vocal folds can displace them from the optical focus and make the images blurry. Suturing the posterior part of the larynx may cause an asymmetry in vocal fold postures, which can cause differences between the strain output for the left and right folds. Suturing is performed to prevent air leakage from the posterior part of the larynx and to guide the air to the glottis. However, the initial strains applied on the vocal folds by suturing could be different from one larynx to another.

Significant differences were observed between the results of this study and those of one using a synthetic vocal fold replica.[4] A phase difference between the displacements in the inferior-superior and medial-lateral directions was only observed for porcine vocal folds. That may be because of differences in the mechanical properties and geometry of vocal fold tissue and the rubber model. In contrast to the findings of the present study, no mucosal wave was reported for the rubber model.[4] The variation of the ε_{xx} and ε_{yy} versus flow rate differs between the rubber model and porcine vocal folds. Because of large values of initial strain in the anterior-posterior direction, vocal folds are under tensile strain during fully closed and fully open state; however, according to Figure 5 in the study by Spencer et al,[4] the rubber model experienced compression in the closed state.

Acknowledgments

This work was supported by National Institute of Health grant R01-DC005788 (Luc Mongeau, principal investigator). The

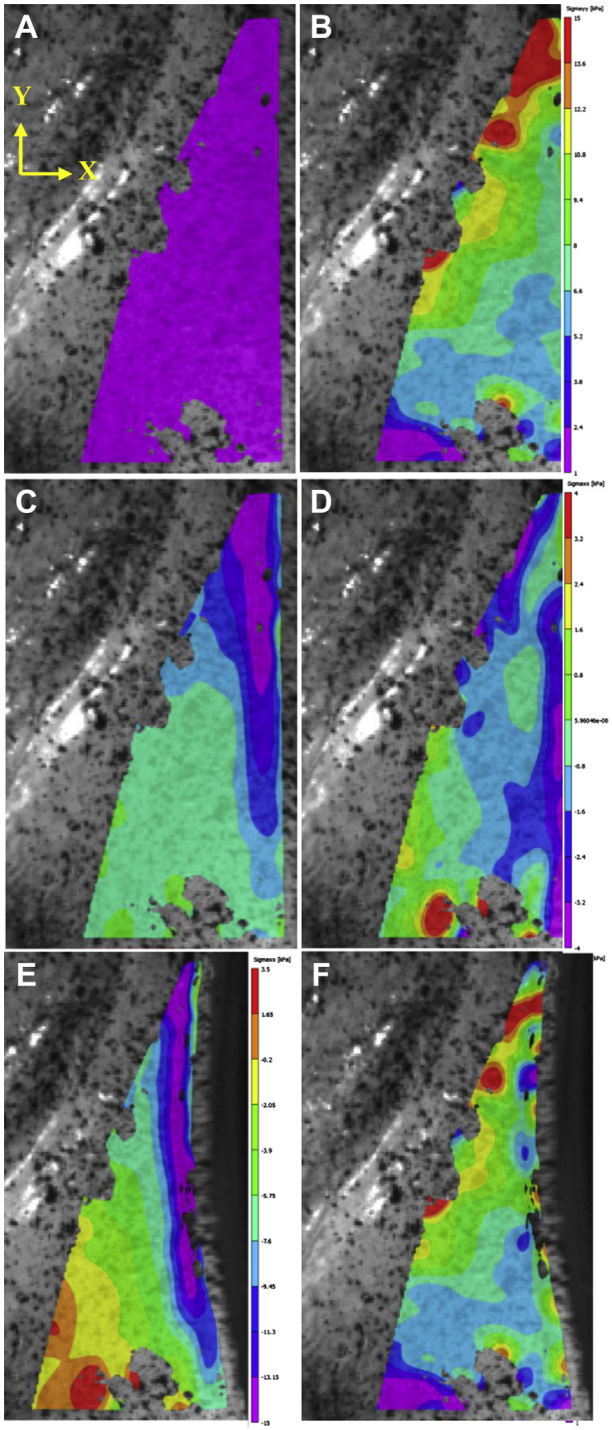

FIGURE 12. **A–B.** Distribution of the normal stress σ_{yy} on deformed surface of vocal fold at closing position based on dynamic strains and dynamic strain with initial strains, respectively. **C–D.** Distribution of the normal stress σ_{xx} on deformed surface of vocal fold at closing position based on dynamic strains and dynamic strain with initial strains, respectively. **E.** Distribution of the normal stress σ_{xx} on deformed surface of vocal fold at opening position. **F.** Distribution of the normal stress σ_{yy} on deformed surface of vocal fold at opening position.

authors thank Dr. Fariborz Alipour (The University of Iowa) for his comments and suggestions on the preparation of the porcine larynges. The authors also thank Mr. Alfred Chan (McGill University) for his assistance in building the setup.

REFERENCES

1. Johns MM. Update on the etiology, diagnosis, and treatment of vocal fold nodules, polyps, and cysts. *Curr Opin Otolaryngol Head Neck Surg*. 2003; 11:456–461.
2. Roy N, Merrill RM, Gray SD, Smith EM. Voice disorders in the general population: prevalence, risk factors, and occupational impact. *Laryngoscope*. 2005;115:1988–1995.
3. Gray S, Titze I. Histologic investigation of hyperphonated canine vocal cords. *Ann Otol Rhinol Laryngol*. 1988;97:381–388.
4. Spencer M, Siegmund T, Mongeau L. Determination of superior surface strains and stresses, and vocal fold contact pressure in a synthetic larynx model using digital image correlation. *J Acoust Soc Am*. 2008;123:1089–1103.
5. Jiang JJ, Titze IR. Measurement of vocal fold intraglottal pressure and impact stress. *J Voice*. 1994;8:132–144.
6. Verdolini K, Chan R, Titze IR, Hess M, Bierhals W. Correspondence of electroglottographic closed quotient to vocal fold impact stress in excised canine larynges. *J Voice*. 1998;12:415–423.
7. Jiang JJ, Shah AG, Hess MM, Verdolini K, Banzali FM, Hanson DG. Vocal fold impact stress analysis. *J Voice*. 2001;15:4–14.
8. Chen LJ, Mongeau L. Verification of two minimally invasive methods for the estimation of the contact pressure in human vocal folds during phonation. *J Acoust Soc Am*. 2011;130:1618–1627.
9. Hess MM, Verdolini K, Bierhals W, Mansmann U, Gross M. Endolaryngeal contact pressures. *J Voice*. 1998;12:50–67.
10. Verdolini K, Hess MM, Titze IR, Bierhals W, Gross M. Investigation of vocal fold impact stress in human subjects. *J Voice*. 1999;13:184–202.
11. Gunter HE, Howe RD, Zeitels SM, Kobler JB, Hillman RE. Measurement of vocal fold collision forces during phonation: methods and preliminary data. *J Speech Lang Hear Res*. 2005;48:567–576.
12. Gunter HE. A mechanical model of vocal-fold collision with high spatial and temporal resolution. *J Acoust Soc Am*. 2003;113:994–1000.
13. Tao C, Jiang JJ, Zhang Y. Simulation of vocal fold impact pressures with a self-oscillating finite-element model. *J Acoust Soc Am*. 2006;119: 3987–3994.
14. Helm JD, McNeill SR, Sutton MA. Improved three-dimensional image correlation for surface displacement measurement. *Opt Eng*. 1996;35: 1911–1920.
15. Miri AK, Barthelat F, Mongeau L. Effects of dehydration on the viscoelastic properties of vocal folds in large deformations. *J Voice*. 2012;26: 688–697.
16. Alipour F, Jaiswal S. Glottal airflow resistance in excised pig, sheep, and cow larynges. *J Voice*. 2009;23:40–50.
17. Alipour F, Jaiswal S. Phonatory characteristics of excised pig, sheep, and cow larynges. *J Acoust Soc Am*. 2008;123:4572–4581.
18. Chu T, Ranson W, Sutton M. Applications of digital-image-correlation techniques to experimental mechanics. *Exp Mech*. 1985;25:232–244.
19. Berry D, Montequin D, Tayama N. High-speed digital imaging of the medial surface of the vocal folds. *J Acoust Soc Am*. 2001;110: 2539–2547.
20. Boessenecker A, Berry DA, Lohscheller J, Eysholdt U, Doellinger M. Mucosal wave properties of a human vocal fold. *Acta Acust Acust*. 2007; 93:815–823.
21. Miri AK, Mongrain R, Chen LX, Mongeau L. Quantitative assessment of the anisotropy of vocal fold tissue using shear rheometry and traction testing. *J Biomech*. 2012;45:2943–2946.
22. Miri AK, Heris HK, Tripathy U, Wiseman PW, Mongeau L. Microstructural characterization of vocal folds toward a strain-energy model of collagen remodeling. *Acta Biomaterialia*. 2013;9:7957–7967.